Article

Not peer-reviewed version

Exploring the Impact of *Onobrychis cornuta* and *Veratrum lobelianum* Extracts on *C. elegans*: Implications for MAPK Modulation, Germline Development, and Antitumor Properties

Qinghao Meng , Nishit Pathak , Xiaojing Ren , Robert P. Borris , Hyun-Min Kim *

Posted Date: 4 December 2023

doi: 10.20944/preprints202312.0154.v1

Keywords: herbal extracts; *O. cornuta*; *V. lobelianum*; DNA repair; meiosis; linoleic acid; germline development; medicinal plants

Article

Exploring the Impact of *Onobrychis cornuta* and *Veratrum lobelianum* Extracts on *C. elegans*: Implications for MAPK Modulation, Germline Development, and Antitumor Properties

Qinghao Meng [1], Nishit Pathak [1], Ren Xiaojing [1] and Robert P. Borris [1] and Hyun-Min Kim [2,*]

[1] School of Pharmaceutical Science and Technology, Tianjin University, 300072 China, 2 Division of Natural and Applied Sciences, Duke Kunshan University, Kunshan 215316, China

* Correspondence: hm.kim@duke.edu; Phone: +86 051233657038

Abstract: In an era of increasing interest in the potential health benefits of medicinal foods, the need to assess their safety and potential toxicity remains a critical concern. While these natural remedies have garnered substantial attention for their therapeutic potential, a comprehensive understanding of their effects on living organisms is essential. We examined 316 herbal extracts to determine their potential nematocidal attributes in *Caenorhabditis elegans*. Approximately 16% of these extracts exhibited the capacity to induce diminished survival rates and larval arrest, establishing a correlation between larval arrest and overall worm viability. Certain extracts led to an unexpected increase in male nematodes, accompanied by a discernible reduction in DAPI-stained bivalent structures and perturbed meiotic advancement, thereby disrupting the conventional developmental processes. Notably, *Onobrychis cornuta* and *Veratrum lobelianum* extracts activated a DNA damage checkpoint response via the ATM/ATR and CHK-1 pathways; hindering germline development. Our LC–MS analysis revealed jervine in *V. lobelianum* and nine antitumor compounds in *O. cornuta*. Interestingly, linoleic acid replicated phenotypes induced by *O. cornuta* exposure, including an increased level of pCHK-1 foci, apoptosis, and the MAPK pathway. We observed that mutants in the MAPK pathway suppressed the reduction in worm survival, emphasizing its role in survivability, meiotic progression, and DNA damage checkpoint-mediated apoptosis. This study reveals complex interactions between herbal extracts and *C. elegans* processes, shedding light on potential antitumor effects and mechanisms. The findings provide insights into the complex landscape of herbal medicine's impact on a model organism, offering implications for broader applications.

Keywords: *O. cornuta; V. lobelianum*; DNA repair; meiosis; linoleic acid; germline

Introduction

Medicinal foods are a rapidly growing market with an expected annual size of USD 2.1 billion, projected to expand at 5.2% from 2022 to 2030 (1). Despite their effectiveness, it is important to note that many herbs can be toxic and lead to side effects. Moreover, numerous herbs have not undergone thorough analytical examination and have not received approval from the Food and Drug Administration (FDA) for use as medicine. Consequently, understanding how herbs function and the potential risks associated with their usage becomes crucial.

To assess the potential toxicity of herbal drugs, various model systems have been employed. The utilization of *C. elegans* offers several advantages due to its simplistic system that allows the comprehension of complex processes (2-4). With high genetic homology (60-80%) to humans, conserved major biological pathways, and the availability of numerous genetic tools such as transgenic models, gene knockouts, and RNAi depletions, *C. elegans* serves as a valuable multicellular animal model for studying human diseases and aging (5, 6). Moreover, its substantial brood size (~300 progeny), short lifespan, and range of behavioral phenotypes provide additional benefits for drug screening while minimizing maintenance costs (7). The transparent skin of *C. elegans* and larger

 doi:10.20944/preprints202312.0154.v1

germline volume also offer advantages for studying meiotic progression. Due to these attributes, *C. elegans* has contributed to numerous significant discoveries in aging research (8)

In recent studies, *C. elegans* has been utilized to explore the effects of herbal extracts. For instance, rosemary flower-derived phenolic compositions were found to alleviate oxidative stress and extend lifespan (9). Additionally, *E. ulmoides* and *C. chinensis* extracts enhanced worm survival under heat stress and exposure to pathogens (10). Ayurvedic herbal extracts displayed neuroprotective and protein aggregation-mitigating effects, potentially beneficial for alleviating symptoms of Parkinson's disease (11).

In this study, we investigated 316 herbal extracts for potential antitumor properties in *C. elegans*. Some (~16%) of the extracts exhibited reduced survival and larval arrest/lethality, indicating that larval arrest plays a role in determining worm viability. Surprisingly, a small but significant portion of herb extracts demonstrated a high incidence of males (HIM), a reduced number of DAPI-stained bodies, and faulty meiotic progression, indicating that certain worms also undergo aberrant meiotic development upon herbal treatment. Interestingly, some herbal extracts triggered a response from the DNA damage checkpoint. When worms were treated with *O. cornuta* and *V. lobelianum*, a DNA damage checkpoint response was activated via the ATM/ATR and CHK-1 pathways and was accompanied by impaired germline development. These findings suggest that both *O. cornuta* and *V. lobelianum* extracts hinder the process of DNA damage repair.

We further examined whether compounds in *O. cornuta* and *V. lobelianum* contribute to their antitumor properties. To delve deeper into the composition of the two herbal extracts, we conducted an analysis using LC–MS. Consistent with a previous report, jervine was identified in the *V. lobelianum* extract. Surprisingly, the *O. cornuta* extract revealed the presence of nine known antitumor compounds. The *O. cornuta* extract and the five major compounds found in *O. cornuta* exhibit upregulation of the MAPK kinase components MEK-2 and SOS-1. Moreover, linoleic acid further mimicked most of the phenotypes exhibited in *O. cornuta,* including increased levels of pCHK-1 and apoptosis. Additionally, mutants defective in the MAPK pathway suppressed the phenotypes observed in *O. cornuta* exposure, suggesting that the MAPK pathway is responsible for survivability and DNA damage checkpoint apoptosis.

Results

Herbal Extracts Unveil Nematocidal Potency

We utilized 316 different herbs to prepare herbal extracts and evaluated their cytotoxic effects on the nematode *C. elegans* (Figure 1A and 1B). For herb extraction, we employed solvents - hexane, butanol, and water, denoted as -H, -B, and -A, respectively.

Preprints.org (www.preprints.org) | NOT PEER-REVIEWED | Posted: 4 December 2023 doi:10.20944/preprints202312.0154.v1

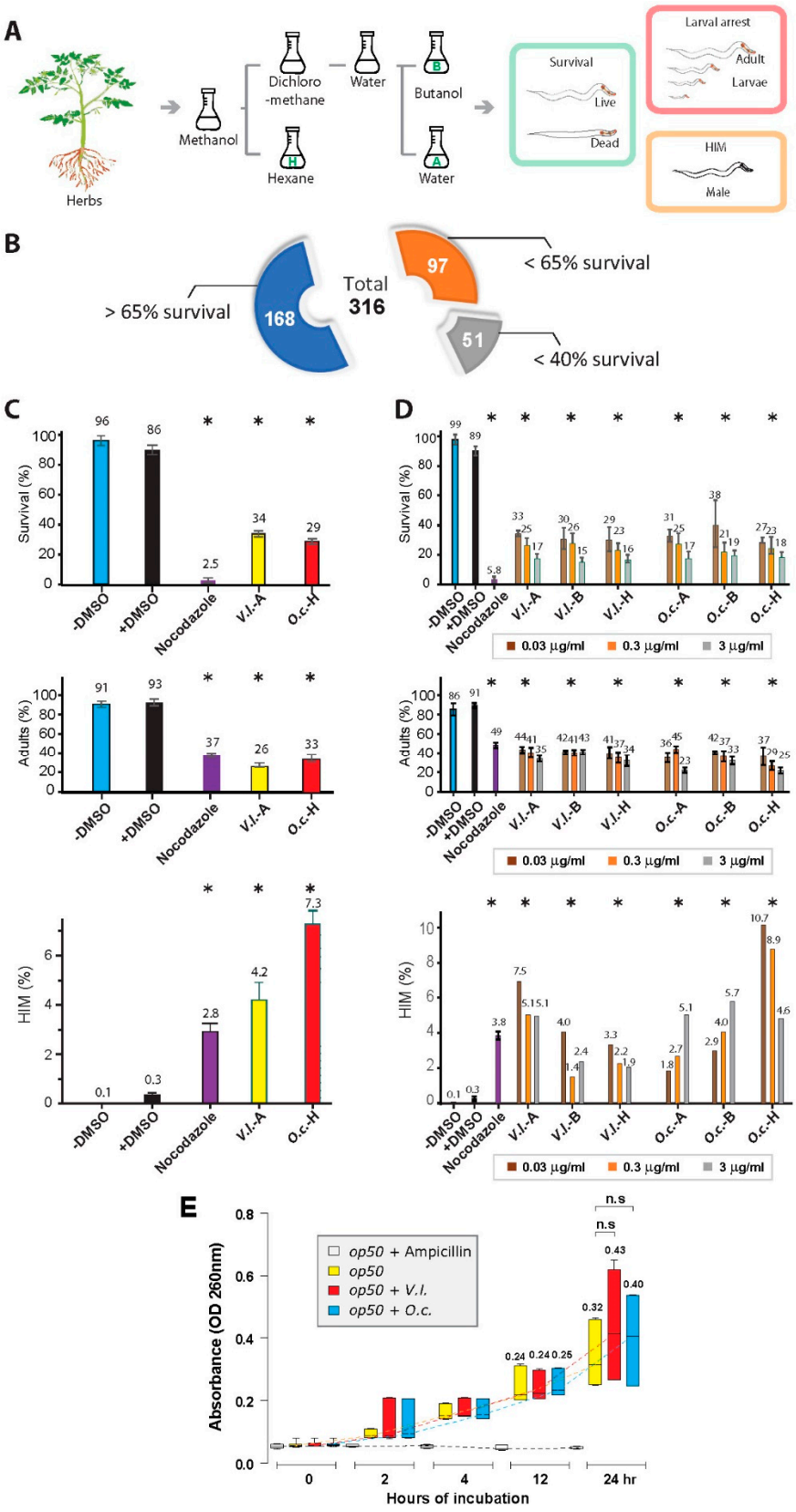

Figure 1. Herb extracts have an inhibitory effect on worm survival and development but do not affect bacterial growth. (A) Experimental workflow depicting the process of extracting compounds from herbs. The extracted compounds were then subjected to phenotypic analysis using the *C. elegans* model system. A one kg sample of the air-dried whole plant of each plant was milled to a coarse powder and extracted with methanol (3 x 6 L). The pooled methanol extract was concentrated in

 doi:10.20944/preprints202312.0154.v1

vacuo to afford a tarry residue. The methanol extract was dissolved in 90% (aqueous) methanol and extracted with n-hexane. The residual hydroalcoholic phase was freed of the solvent *in vacuo*, suspended in water, and then sequentially extracted with dichloromethane and n-butanol (n-BuOH) to afford a gross separation into hexane-, dichloromethane-, butanol-, and water-soluble fractions. Three solvents, hexane, butanol, and water, were designated -H, -B, and -A, respectively. **(B)** The impact of plant extracts on *C. elegans* survival and development overview. A total of 316 (168+97+51) extracts were tested, revealing significant nematocidal effects. Survival (%), adult (%) and HIM (%) of *C. elegans* were monitored after a 24-hour treatment of herb extract and monitored for 48 hours. **(C)** Phenotypic effects of *O. cornuta* and *V. lobelianum* herbal extracts on *C. elegans*. Comparative analysis of distinct herbal extracts, *O. cornuta* (*O.c.*) and *V. lobelianum* (*V.l.*), revealed significant phenotypic outcomes. (Top), Reduced survivability in worms treated with herbal extracts in comparison to the +DMSO control group. The microtubule depolymerizing agent nocodazole was used as a positive control (56). *O.c.*-H: *O. cornuta* - hexane extract; *V.l.*-A: *V. lobelianum* - water extract. P values were determined using the two-tailed Mann–Whitney test. (Middle), Induction of larval arrest and/or lethality in worms exposed to the extracts indicates compromised mitotic growth (% Adults). (Bottom), High incidence in males (HIM) upon herb extract exposure suggests potential sex chromosome mis-segregation and abnormal meiotic development. DMSO and nocodazole were used as controls. P values were determined by the two-tailed Mann–Whitney test. **(D)** Dose-dependent effects of Herb Extracts on Survival, Adult Formation, and HIM Phenotype. Investigation into the dose-dependent relationship between herbal extract concentrations and C. elegans phenotypes. (Top, middle) Survival rates and adult formation were inversely correlated with increasing herbal extract doses. Dose–response trends were consistent across extracts from different solvents (-A, -B, -H). (Bottom), Induction of the HIM phenotype in response to herb extracts. Asterisks indicate statistical significance by the two-tailed t test. **(E)** Evaluation of Herb Extracts' Impact on Bacterial Growth. Analysis over 24 hours revealed no significant bacterial growth defect, suggesting that the nematocidal effects were not primarily attributed to compromised bacterial growth.

Almost half of the plant extracts (47%, 148 out of 316 extracts) demonstrated potent nematocidal effects following a 24-hour treatment at 20°C, resulting in less than 65% survival (Figure 1B). Moreover, among these extracts, 51 (16%) exhibited even lower survival rates, falling below 40%, in comparison to a control group treated with DMSO. We directed our attention toward two distinctive herbal extracts, *O. cornuta (O.c.*) and *V. lobelianum (V.l.*), both of which exhibited notable phenotypes (Figure 1C). Comparative analysis revealed that both herbal extracts exhibited significantly reduced survivability when compared to the nontreated control group (86 vs 34 in +DMSO and *V.l.*-A, P=0.00003; 86 vs 29 in +DMSO and *O.c.*-H, P=0.0001, as determined by the two-tailed Mann–Whitney test).

Furthermore, worms exposed to these extracts demonstrated either larval arrest and/or lethality (93 vs 26 in +DMSO and *V.l.*-A, P=0.00002; 93 vs 33 in +DMSO and *O.c.*-H, P=0.00003, using the two-tailed Mann–Whitney test). This observation strongly suggests a link between compromised survivability and mitotic growth defects. Notably, both extracts also induced a significant increase in the occurrence of males (HIM phenotype), indicating potential sex chromosome mis-segregation and abnormal meiotic development in the worms (0.3 vs 4.2 in +DMSO and *V.l.*-A, P=0.00005; 0.3 vs 7.3 in +DMSO and *O.c.*-H, P=0.0071, as determined by the two-tailed Mann–Whitney test).

Dose-Dependent Nematocidal Effects of Herbal Extracts: Correlation and Phenotypic Observations

To further validate the nematocidal effects, we investigated whether varying doses of herb extracts correlated with the observed phenotypes of the two herbs. As the dose of the herbal extract increased by tenfold, we observed a corresponding decrease in survivability for both herbal extracts, indicating a clear dose-dependent phenomenon (Figure 1D). For instance, in *V.l.*-A, survivability changed from 33, 25, to 17, and in *O.c.*-H, it changed from 27, 23, to 18 for concentrations of 0.03, 0.3, and 3 ng/ml, respectively.

Remarkably, this dose dependency was evident across extracts obtained from three solvents (A, B, H). Similarly, the number of adults also declined with increasing herb concentrations, indicating

 doi:10.20944/preprints202312.0154.v1

that the herb extracts indeed impeded mitotic growth (Figure 1D). For instance, in *V.l.*-A, the number of adults shifted from 44, 41, to 35, and in *O.c.*-H, it shifted from 37, 29, to 25 for concentrations of 0.03, 0.3, and 3 ng/ml, respectively.

C. elegans reproduce through self-fertilization. Errors during the separation of sex chromosomes in cell division can lead to offspring with abnormal sex chromosome compositions, resulting in an increased incidence of males, known as the HIM (High Incidence of Males) phenotype. This HIM phenotype serves as a crucial indicator for studying the impacts of these factors on sex chromosome segregation, chromosomal abnormalities, and reproductive processes (3, 12).

While we observed the induction of the HIM phenotype with all six types of herb extracts, intriguingly, we did not discern a distinct dose dependency. This suggests that defective sex chromosomal segregation was not directly correlated with the dosages of the herb extracts (Figure 1D). For example, in *V. lobelianum*-A, the HIM phenotype was observed at 7, 5.1, and 5.1, and in *O.c.*-H, it was observed at 10.7, 8.9, and 4.6 for concentrations of 0.03, 0.3, and 3 ng/ml, respectively.

Impact of Herb Extracts on Nematode Survival and Bacterial Growth

The decreased survival of *C. elegans* might arise from poor bacterial growth rather than a direct correlation between worms and herbs. To explore this possibility, we investigated whether herb extracts inhibit bacterial growth. No significant bacterial growth defect was observed in the case of the two herbs over 24 hours of incubation, implying that bacterial growth did not play a crucial role in the nematocidal effects (Figure 1E, $P<0.1248$ in *op50* and *op50 +V. l.*; $P < 0.1994$ in *op50* and *op50 +O.c.*).

Our data indicate that both *V. lobelianum* and *O. cornuta* extracts hinder survivability, larval growth, and sex chromosomal segregation. The dosage of herb extracts correlates with decreased survivability and larval arrest.

Herbal extracts cause defective germline progression

The nuclei within *C. elegans* are spatially and temporally arranged along germline progression, with actively dividing mitotic nuclei occupying the distal end of the premeiotic tip (PMT). As cells move away from the PMT, they enter meiotic prophase, commencing from the transition zone, where nuclei assume a crescent shape (3, 13).

Given that both herb extracts induced defective meiotic progression, we investigated how herbal extracts may affect germline development. We examined adult hermaphrodites that were dissected and stained with DAPI, and we scored the presence of the premeiotic tip (PMT), transition zone (TZ), and pachytene stages. While the nuclei in the control group were precisely ordered during germ cell development, worms exposed to herbal extracts exhibited an increase in gaps between nuclei in the PMT-TZ and pachytene stages, indicating aberrant progression of germline nuclei (Figure 2A)

Preprints.org (www.preprints.org) | NOT PEER-REVIEWED | Posted: 4 December 2023 doi:10.20944/preprints202312.0154.v1

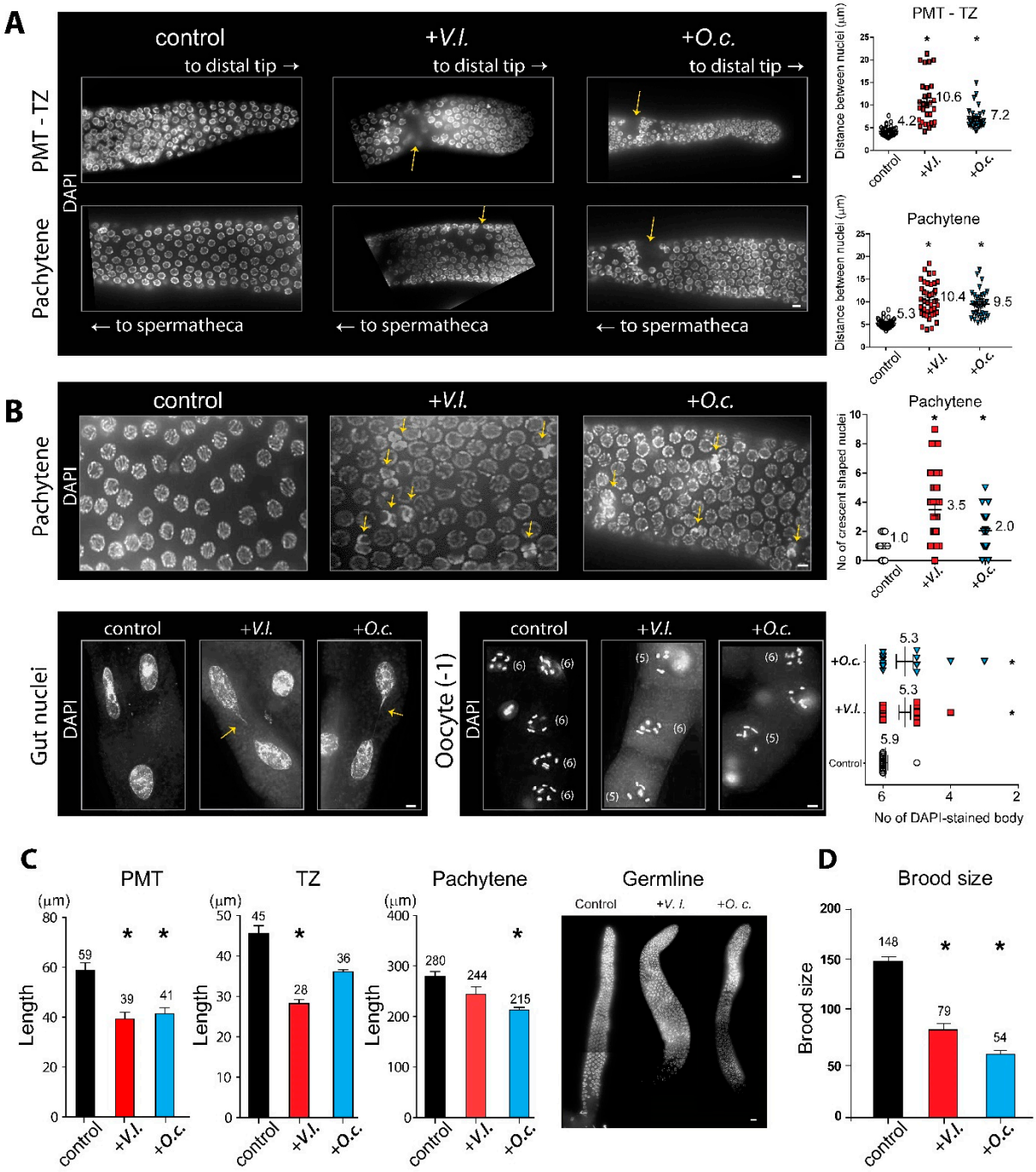

Figure 2. Defective germline development induced by herbal extracts. (A) Nuclei arrangement during germline development in control and herb extract-exposed *C. elegans* hermaphrodites. Exposure to *V. lobelianum* (+*V.l.*) and *O. cornuta* (+*O.c.*) extracts resulted in increased gaps indicated by arrows between nuclei in the premeiotic tip-transition zone (PMT-TZ) and pachytene stages. The distances between adjacent nuclei were significantly greater in herb extract-treated worms than in control worms. Asterisks indicate statistical significance by the two-tailed Mann–Whitney test. Bar=2 μm. **(B)** Aberrant transition from mitosis to meiosis and chromatin bridge formation. Herbal extract exposure led to aggregates of crescent-shaped nuclei (top row) and chromatin bridges in mitotic gut cells (bottom left). Additionally, herb extract-exposed worms exhibited reduced DAPI-stained bodies during diakinesis (bottom right), indicating a faulty DNA recombination process. Asterisks indicate statistical significance by the two-tailed Mann–Whitney test. Bar=2 μm. **(C)** Decreased length of PMT, TZ, and pachytene stages. *V. lobelianum* and *O. cornuta* extracts led to reduced lengths of the PMT, TZ, and pachytene stages compared to the control. Asterisks indicate statistical significance by the two-tailed Mann–Whitney test. Right, the overall shape of the germline upon herb extract exposure.

 doi:10.20944/preprints202312.0154.v1

Bar=10 μm. **(D)** Impaired fertility due to defective germline development. Exposure to herbal extracts resulted in a significant reduction in the number of progeny produced by hermaphrodite worms over a span of four days. Asterisks indicate statistical significance by the two-tailed Mann–Whitney test. All experiments were performed on *C. elegans* hermaphrodites. Data are presented as the mean ± SEM.

The quantification of the distance between adjacent nuclei further confirmed that *V. lobelianum* and *O. cornuta* extracts induced significant spatial disorganization of nuclei both in the PMT-TZ and pachytene stages (Figure 2A). In the PMT-TZ stage, the distances were 4.2 vs 10.6 μm in the control and +*V.l.*, P<0.0001; 4.2 vs 7.2 μm in the control and +*O.c.*, P<0.0001. In the pachytene stage, the distances were 5.3 vs 10.4 μm in the control and +*V.l.*, P<0.0001; 5.3 vs 9.5 μm in the control and +*O.c.*, P<0.0001, as determined by the two-tailed Mann–Whitney test.

In *C. elegans*, crescent-shaped nuclei indicate the transition from the mitotic to meiotic stages (3, 14). Both herb extracts resulted in aggregates of two or more crescent-shaped nuclei during the pachytene stages, whereas the control group did not, implying that the defective transition from mitosis to meiosis persisted from the TZ to pachytene stages upon herb extract treatment (Figure 2B, top row, 1.0 vs 3.5 μm in control and +*V.l.*, P= 0.0001; 1.0 vs 2.0 μm in control and +*O.c.*, P=0.0083 by two-tailed Mann–Whitney test).

Consistently, we observed a reduction in the length of the PMT, which is occupied by mitotic nuclei, in *V. lobelianum* and *O. cornuta* compared to the control groups (Figure 2C). The length decreased by 34% (59 vs 39 μm for the control and +*V.l.*, P=0.0017; 59 vs 41 μm for the control and +*O.c.*, P=0.0021, determined by a two-tailed t test. Similarly, *V. lobelianum* and *O. cornuta* led to a decrease in the length of the TZ or pachytene stages, where meiotic progression occurs (45 vs 28 in the control and +*V.l.*, P=0.0003; 45 vs 36 in the control and +*O.c.*, P=0.076; 280 vs 244 in the control and +*V.l.*, P=0.076; 280 vs 215 in the control and +*O.c.*, P=0.0004, as determined by the two-tailed Mann–Whitney test.

In line with larval lethality, we also observed defective mitotic progression in mitotic gut cells (Figure 2B, bottom left). *V. lobelianum* and *O. cornuta* extracts frequently led to the formation of a chromatin bridge, which manifests as a string of chromatin connecting two segregating chromosomes during anaphase or linking daughter nuclei in cytokinesis. In contrast, the untreated control group did not exhibit such a chromatin bridge. This finding indicates the failure to eliminate replication or recombination intermediates (15, 16).

During the diakinesis stage of the germline, six bivalents held together by chiasmata, corresponding to six pairs of homologous chromosomes, become visible (3). However, exposure to the herb extracts failed to form six pairs of homologous chromosomes, resulting in five DAPI-stained bodies in both the *V. lobelianum* and *O. cornuta* groups, indicative of defective DNA repair (Figure 2B, bottom right). The counts were 5.9 vs 5.3 in the control and +*V.l.*, P=0.0045; 5.9 vs 5.3 in the control and +*O.c.*, P=0.0035 (17).

Given the reduction in survival exhibited by the herbal extracts, we conducted further tests to determine whether the defective germline progression resulted in a reduced brood size. We counted the number of progeny laid by single hermaphrodite worms starting from L4 and over a span of four days. We found that both extracts resulted in a significant reduction in fertility, further supporting the idea of defective meiotic development induced by the two herb extracts (Figure 2D). The counts were 148 vs 79 in the control and +*V.l.*, P<0.0001; 148 vs 54 in the control and +*O.c.*, P<0.0001).

These observations illustrate how herbal extracts disrupt the orderly progression of the germline, ultimately culminating in reduced fertility. Exposure to these herbal extracts disrupts the usual progression, leading to an increase in gaps between nuclei during the PMT-TZ and pachytene stages. Additionally, the extracts result in aggregates of crescent-shaped nuclei, indicative of a faulty mitotic-to-meiotic transition. This is also supported by a reduction in the PMT, TZ, and pachytene stages, further affecting meiotic progression. Chromatin bridges in mitotic gut cells indicate defective mitotic progression, while the inability to form six pairs of homologous chromosomes during diakinesis suggests faulty DNA repair. These cumulative defects ultimately lead to a reduction in brood size, underscoring the adverse impact of herbal extracts on germline development and fertility in *C. elegans*. In summary, our observations compellingly suggest that *V. lobelianum* and *O. cornuta*

 doi:10.20944/preprints202312.0154.v1

extracts disrupt proper germline development and mitotic cell growth, consequently leading to compromised fertility.

Herbal extracts activate DNA damage checkpoint pathways: ATM, ATR, CHK1, and apoptosis.

The DNA damage response is a signaling pathway that coordinates cellular reactions to DNA lesions, triggering a series of responses, such as DNA damage repair, apoptosis, and cell cycle arrest (18, 19). This intricate pathway is regulated by two kinases, ATM and ATR, each with distinct DNA damage specificities. Often, they collaborate to modulate downstream processes of CHK1 (Figure 3A, (20)). ATM and ATR can both activate CHK1 either directly or indirectly through intermediate kinases. The activation of CHK1 subsequently initiates downstream events that promote DNA repair, halt cell cycle progression, and uphold genome stability in the face of DNA damage or replication stress.

Preprints.org (www.preprints.org) | NOT PEER-REVIEWED | Posted: 4 December 2023 doi:10.20944/preprints202312.0154.v1

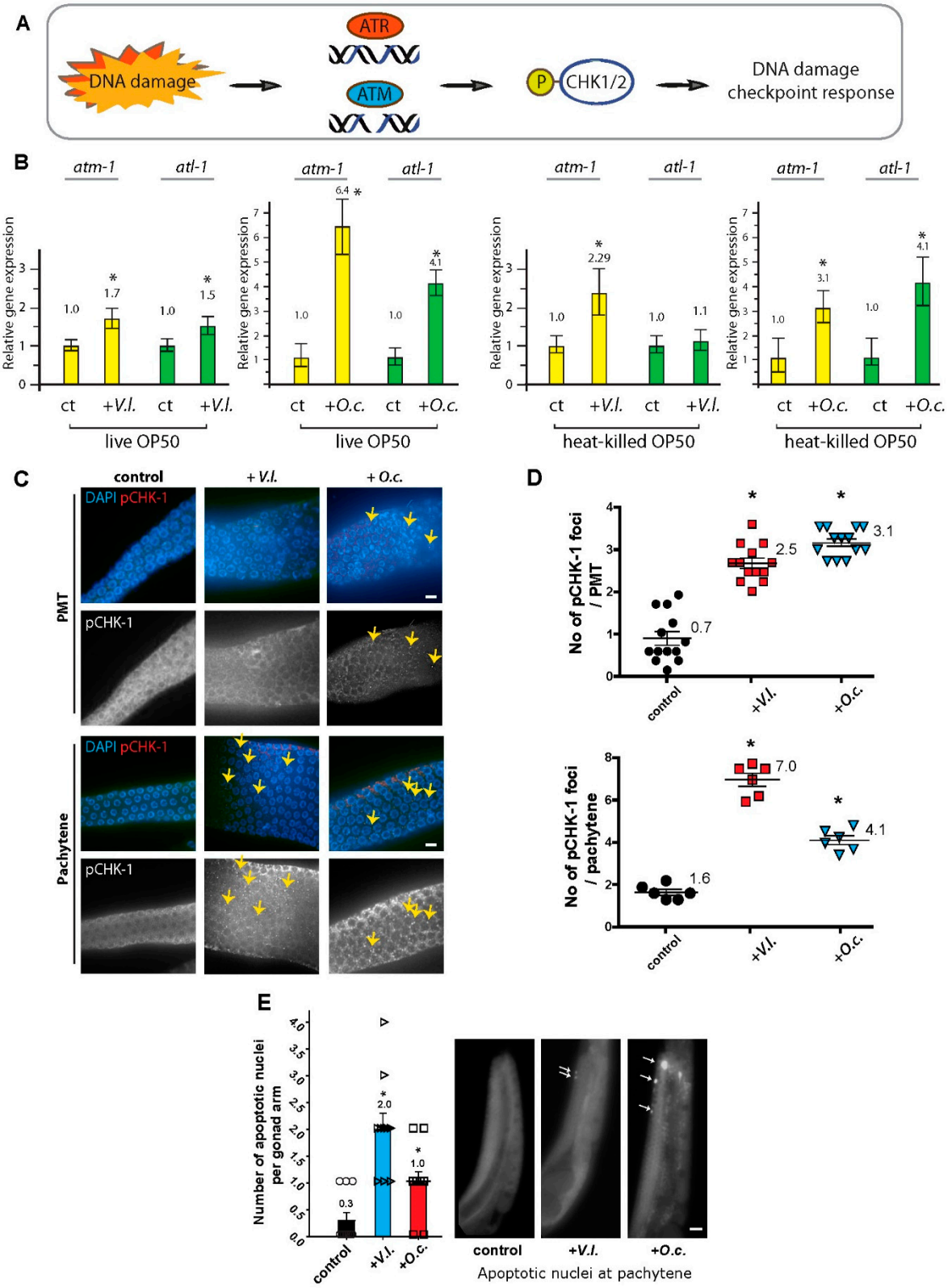

Figure 3. Exposure to herbal extracts of *V. lobelianum* and *O. cornuta* activates the DNA damage response pathway in *C. elegans*, resulting in increased levels of key DNA damage checkpoint components and phosphorylated CHK-1. (A) ATM and ATR kinases collaboratively regulate downstream CHK-1 processes in the intricate DNA damage response pathway, playing essential roles in DNA damage repair. (B) Exposure to herbal extracts leads to increased expression of ATM-1 and ATL-1, validating activation of the DNA damage response pathway. Gene expression levels between live and autoclaved OP50 were comparable, indicating that the nematocidal effects attributed to the herbal extracts may not be influenced by bacterial metabolism. Asterisks indicate statistical

 doi:10.20944/preprints202312.0154.v1

significance by the two-tailed Mann–Whitney test. (C) Elevated pCHK-1 foci observed in germlines underscores the active DNA damage response following exposure to herbal extracts, confirming checkpoint activation. Bar=2 μm. (D) Quantification of the number of pCHK-1 foci presented in (C). Asterisks indicate statistical significance by the two-tailed Mann–Whitney test. (E) The pachytene stage revealed an increased level of apoptosis, suggesting that unrepaired DNA damage triggers checkpoint activation and subsequent apoptosis in the germline. Asterisks indicate statistical significance by the two-tailed Mann–Whitney test. Bar=20 μm.

The defects in DNA damage repair indicate that the herb extracts trigger the activation of the DNA damage checkpoint (Figure 2B). To corroborate the heightened expression of DNA damage checkpoint response pathways, we assessed the levels of ATM-1 (homolog of mammalian ATM), ATL-1 (homolog of mammalian ATR), and pCHK-1 (homolog of mammalian CHK1), the active form of CHK-1. Upon exposure to *V.l.*, there was an increase in the expression of *atm-1* and *atl-1* (Figure 3B), with 1.7-fold and 1.5-fold induction, respectively (P=0.0026 and P=0.0007). Similarly, *O. cornuta* treatment led to elevated expression of these two pivotal DNA damage checkpoint components, signifying the activation of the DNA damage response due to herbal treatment (with a 6.4-fold induction in *atm-1* and a 4.1-fold induction in *atl-1* expression, P=0.00022 and P=0.00029, respectively).

In line with the mRNA expression profile, elevated levels of pCHK-1 foci were observed in the pachytene stage of germlines, indicating an active DNA damage response following exposure to herbal extracts (Figure 3C, (19, 21)). The two herb extracts exhibited an induction in the PMT and/or pachytene stage, further confirming the activation of the DNA damage checkpoint and CHK-1 phosphorylation (Figure 3C and 3D, 0.7 vs 2.5 in PMT of *V. lobelianum*, P=0.0121; 0.7 vs 3.1 in PMT of *O.c.*, P=0.0072; 1.6 vs 7.0 in pachytene of *V. lobelianum*, P=0.0004; 1.6 vs 4.1 in pachytene of *O.c.*, P=0.0008).

Moreover, we investigated whether the observed nematocidal phenotypes were contributed by the secondary metabolites produced by *E. coli OP50*. To test this hypothesis, we fed *C. elegans* with heat-killed OP50 and compared its gene expression level to that of live OP50-fed worms. No discernible differences in gene expression were observed between autoclaved and live OP50 in both herbs, indicating that the nematocidal phenotypes observed with herbal extracts were not a result of bacterial metabolism (Figure 3B).

Since unrepaired DNA intermediates can result in apoptosis in pachytene nuclei (21, 22), we further investigated DNA damage-induced apoptosis in the germline. In comparison to the untreated control group, which rarely displayed nuclei highlighted by acridine orange staining, both *V. lobelianum* and *O. cornuta* treatments showed an increase in the number of acridine orange-stained nuclei during pachytene (Figure 3E, 0.3 vs 2.0 in control and *V.I.*, P<0.0001; 0.3 vs 1.0 in control and *O.c.*, P=0.0150).

Collectively, our findings demonstrate that exposure to herbal extracts heightened the expression of key components in the ATM/ATR-dependent DNA damage checkpoint pathway and elevated levels of phosphorylated CHK-1, signifying activation of the DNA damage response. These observations strongly indicate that unrepaired DNA damage persists and triggers the DNA damage checkpoint, ultimately leading to increased apoptosis in the *C. elegans* germline. Altogether, the herbal extracts of *V. lobelianum* and *O. cornuta* activate the DNA damage response pathway in *C. elegans*, leading to an increased level of DNA damage-mediated apoptosis.

LC–MS analysis identified anticancer compounds

Herbal extracts encompass a broad spectrum of plant chemicals. To gain insights into the specific compounds contributing to the DNA damage pathway, we conducted LC–MS (liquid chromatography–mass spectrometry) analysis to identify the biologically active constituents of these extracts. Our analysis of the herbal extract from *V. lobelianum* and *O. cornuta* unveiled the presence of more than 19 and 13 compounds, respectively. Among the major components identified were flavonoids and terpenoids (as shown in Table 1, Figure 4, and Additional file 1).

Table 1. Phytochemical composition of *Veratrum lobelianum* and *Onobrychis cornuta.*

 doi:10.20944/preprints202312.0154.v1

No.	Compound	Rt	$[M+H]^+$	Fragments	Herbs	Types
1	Luteolin-7-O-Rucoside	12.091	**595.1659**	286.0477, 301.0713, 463.1224	*V.l. and O.c.*	Flavonoids
2	Thymol	20.594	**151.1118**	77.0408, 91.0574, 105.0714, 107.0540	*V.l. and O.c.*	Terpenoids
3	Dihydrocarvone	26.597	**153.1275**	152.1122	*V.l. and O.c.*	Terpenoids
4	Carvyl acetate	17.201	**195.135**	153.1283	*V.l. and O.c.*	Terpenoids
5	Menthyl Acetate	27.991	**199.1697**	144.0785, 111.1197, 55.0596, 69.0730	*V.l. and O.c.*	Terpenoids
6	Luteolin	1.36	**287.0527**	168.0056, 140.0109	*V.l. and O.c.*	Flavonoids
7	2,4,3',5'-tetrahydroxyindole	21.186	**245.0784**	228.0723, 180.9145, 140.9176	*V.l. and O.c.*	Phenolic compounds
8	Pilloin	1.125	**315.0803**	182.0429	*V.l. and O.c.*	Carotenoid
9	Linoleic acid	28.325	**281.2491**	248.9901, 151.0287	*V.l. and O.c.*	Fatty acids
10	Homoplantain	12.761	**463.1233**	301.0711, 286.0476	*V.l. and O.c.*	Alkaloids
11	Resveratrol	23.73	**229.086**	151.0394	*V.l.*	Phenolic compounds
12	Diosmetin	12.762	**301.0705**	286.0476, 168.0044	*V.l.*	Lignin
13	Ferruginol	27.55	**287.2358**	173.1332, 93.0721	*V.l.*	Prostaglandins
14	Tilianin	18.678	**447.1294**	294.1053, 259.1366, 105.0362	*V.l.*	Flavonoids
15	Vitexin	12.589	**433.1126**	286.0474	*V.l.*	Flavonoids
16	Vitexin-2 "- O-rhamnoside	10.538	**579.1712**	301.1366, 285.0770	*V.l.*	Flavonoids
17	Vitexin-4 "- O-glucoside	12.091	**595.1659**	463.1240, 301.0713, 286.0477	*V.l.*	Flavonoids
18	Naringin	13.299	**581.1859**	273.0768	*V.l.*	Flavonoids
19	Jervine	11.59	**426.3005**	313.2138	*V.l.*	Alkaloids
20	Sugiol	23.15	301.2165	259.1685, 163.0752	*O.c.*	Terpenoids
21	Dihydrotanshinone I	**22.663**	**279.0934**	152.1122	*O.c.*	Tanshiones
22	Aucubin	26.472	347.1351	216.9976, 129.0189	*O.c.*	Iridoids
23	Pacitaxel	5.34	297.77	279.0874	*O.c.*	Iridoids

The types of phytochemicals were highlighted with different colors.

 doi:10.20944/preprints202312.0154.v1

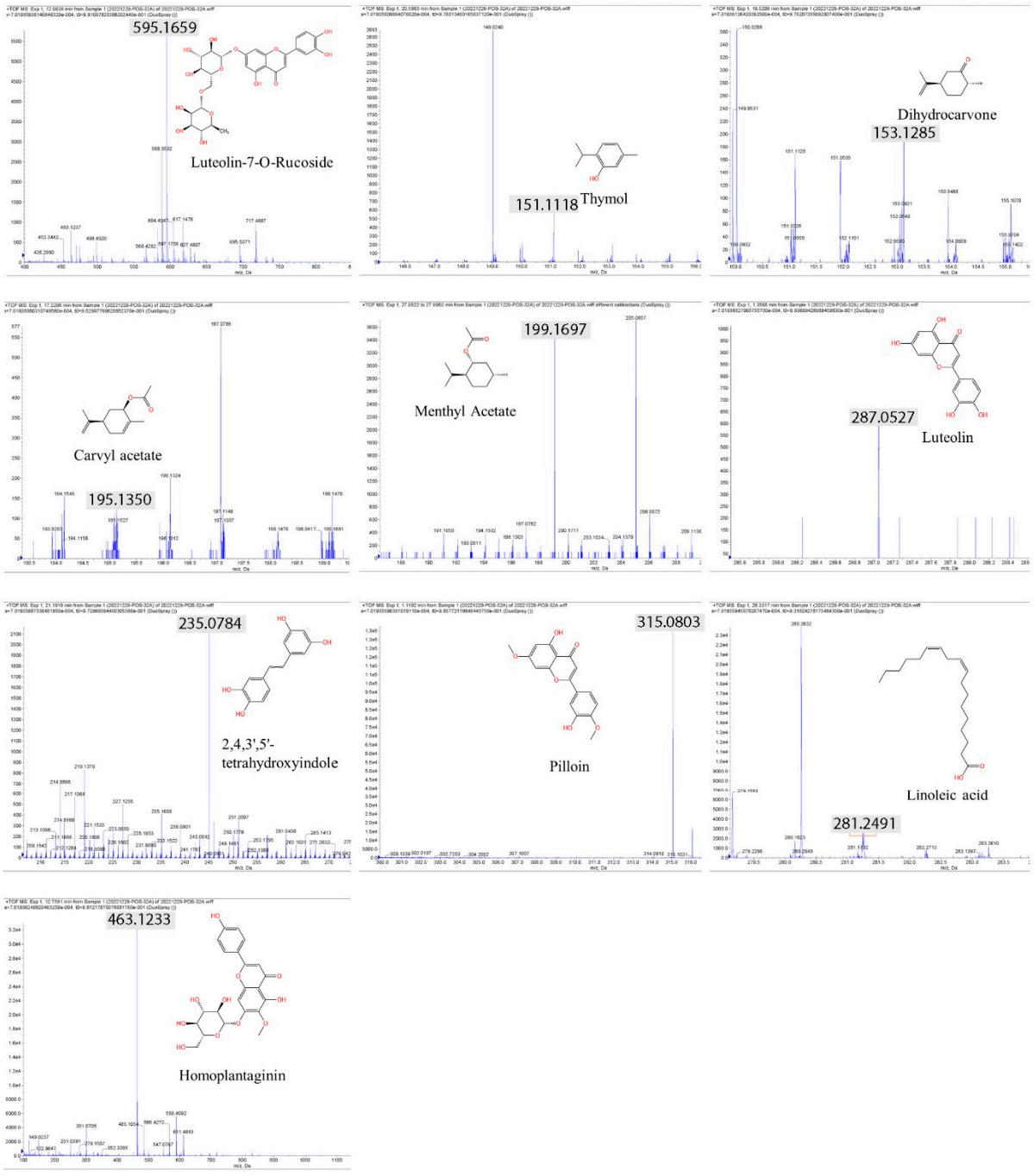

Figure 4. Spectrum of phytochemicals identified in both *V. lobelianum* and *O. cornuta*. Ten compounds were found in both herb extracts. Gray marking and the numbers indicate the predicted fragmentation of compounds provided by Analyst 1.6, an in silico analysis tool. The x-axis in an LC–MS graph represents the mass-to-charge ratio (m/z), which indicates the size and charge of ions. The y-axis represents intensity in counts per second (cps), showing how many ions of a particular m/z are detected.

Common compounds identified in both extracts included luteolin-7-O-ructoside, thymol, dihydrocarvone, carvacrol acetate, methyl acetate, luteolin, 2,4,3′,5′-tetrahydroxystilbene, pilloin, linoleic acid, and homoplantain. Additionally, the extract of *V. lobelianum* contained resveratrol, diosmetin, ferruginol, tilianin, vitexin, vitexin-2″-O-rhamnoside, vitexin-4″-O-glucoside, naringin, and jervine, while the extract of *O. cornuta* contained sugiol, dihydrotanshinone I, aucubin, and paclitaxel. The list of detected compounds is provided in Table 1 and Additional file 1.

 doi:10.20944/preprints202312.0154.v1

V. lobelianum and the Hedgehog pathway

We hypothesized that the compounds present in the herbs may contribute to the observed phenotypes in the herbal extracts. Jervine, a primary alkaloid found in *V. lobelianum* (23, 24), has been identified as an inhibitor of the Hedgehog pathway in nasopharyngeal carcinoma—a crucial cellular pathway involved in cell growth, differentiation, and tissue formation (25-27).

Consistent with findings in human carcinoma studies, the mRNA expression profile indicated that two orthologs of Hedgehog signaling components in *C. elegans* were significantly downregulated upon treatment with the *V. lobelianum* extract (Figure 5A, (28, 29)). This suggests that inhibited Hedgehog signaling might trigger DNA damage checkpoint activation, followed by germline apoptosis (Fig 3C, 3D, and 3E). Specifically, *wrt-1* expression showed a change of 1.06 vs 0.58 in control vs. *V. lobelianum*, with a significance of P=0.0412, and *hog-1* expression displayed a change of 1.11 vs 0.58 in control vs. *V. lobelianum*, with a significance of P=0.0379. However, surprisingly, when jervine was used alone but not as part of the herb extract, it led to the upregulation of the hedgehog signaling pathway (Figure 5B). This indicates a different effect compared to its use within the herb extract. Indeed, unlike the *V. lobelianum* extract, jervine *per se* did not increase the level of pCHK-1 foci or apoptosis (Figure 5C, 1.4 vs 0.6, $P < 0.0001$; Figure 5D, 1.4 vs 1.0, $P = 0.1077$). These observations collectively suggest that the *V. lobelianum* extract induces the DNA damage checkpoint and apoptosis in a manner independent of jervine in the *C. elegans* germline while also compromising the hedgehog pathway.

Preprints.org (www.preprints.org) | NOT PEER-REVIEWED | Posted: 4 December 2023 doi:10.20944/preprints202312.0154.v1

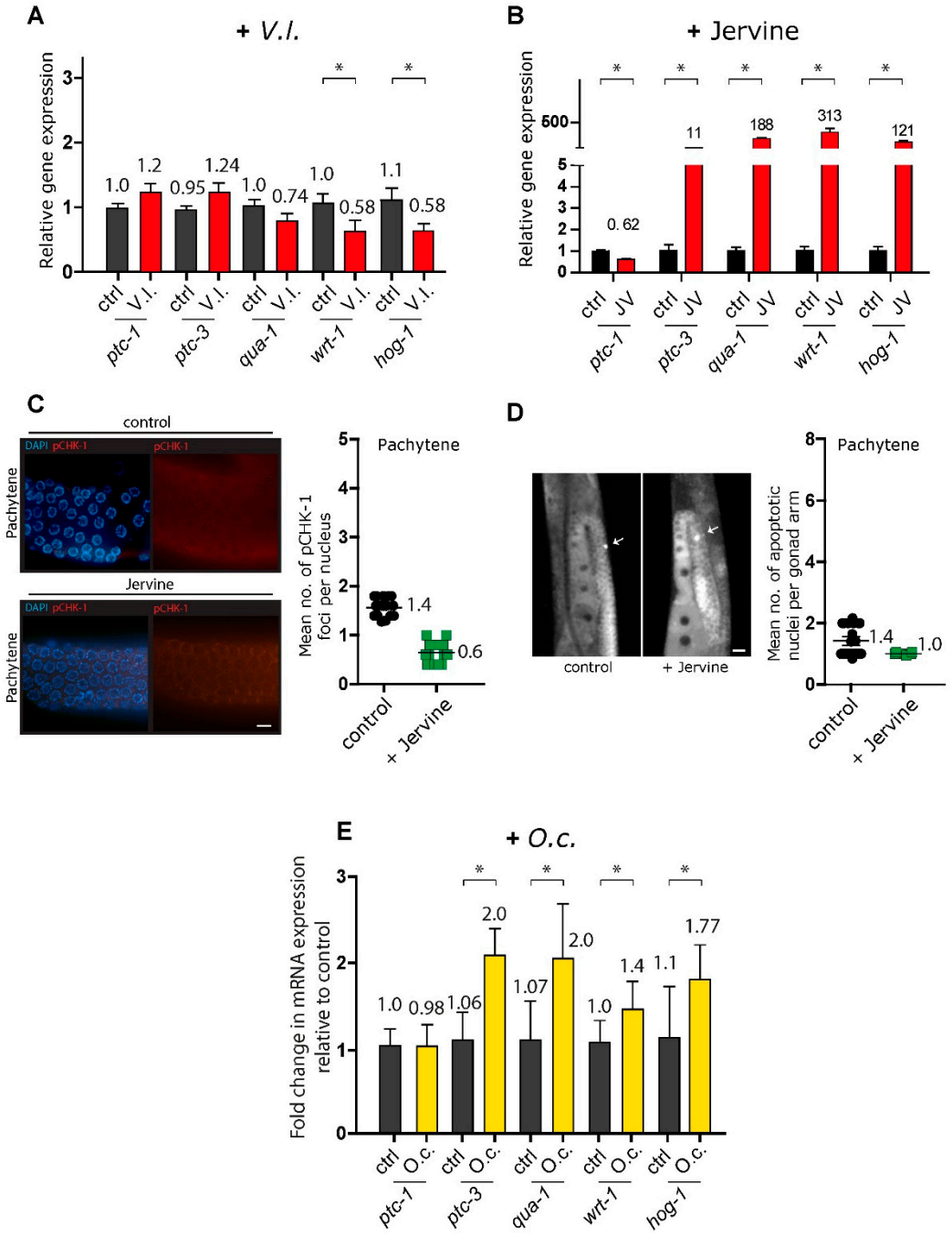

Figure 5. mRNA expression profiles and effects of herbal extracts on DNA damage checkpoint activation, apoptosis, and hedgehog pathway components. (A) mRNA expression profile of hedgehog signaling components in *C. elegans* treated with *V. lobelianum* extract. *wrt-1* and *hog-1* were significantly downregulated. (B) Upregulation of the hedgehog signaling pathway when jervine was used alone. (C) Jervine extract did not increase the number of pCHK-1 foci (1.4 vs 0.6 in control and +jervine, $P < 0.0001$). Bar=2 μm. (D) *V. lobelianum* extract did not induce apoptosis (1.4 vs 1.0 in control and +jervine, $P = 0.1077$). Bar=20 μm. (E) *O. cornuta* extract led to upregulation of the hedgehog pathway components *wrt-1, hog-1, ptc-3, and qua-1*, distinct from *V. lobelianum* extract. Asterisks indicate statistical significance by the two-tailed Mann–Whitney test.

O. cornuta and the MAPK kinase pathway

Similar to *V. lobelianum, O. cornuta* extracts triggered the activation of DNA damage checkpoints, induction of germline apoptosis, and defects in germline development (Figure 2 and 3). However, a

 doi:10.20944/preprints202312.0154.v1

notable distinction emerged: *O. cornuta* extract led to upregulation of several components within the hedgehog pathway, such as *wrt-1* and *hog-1* expression, which were downregulated in the *V. lobelianum* extracts. This suggests distinct mechanisms between the two herbal extracts (Figure 5E, 1.0 vs 1.4 in control and +*O.c.* for *wrt-1* expression, P = 0.0040; 1.1 vs 1.77 in control and +*O.c.* for *hog-1* expression, P = 0.0037; 1.06 vs 2.0 in control and +*O.c.* for *ptc-3* expression, P<0.0001; 1.07 vs 2.0 in control and +*O.c.* for *qua-1* expression, P=0.0005). Consequently, we screened for potential pathways whose expression levels were altered upon exposure to *O.c.*

The mitogen-activated protein kinase (MAPK) pathway is a critical signaling cascade that regulates various cellular processes, including cell proliferation, differentiation, and survival. It involves a series of protein kinases that activate each other sequentially through phosphorylation events. In germline development, the MAPK pathway plays a pivotal role in modulating the progression of germline nuclei through different meiotic stages, ultimately leading to the production of haploid gametes (30, 31).

Surprisingly, the MAPK pathway components *mek-2* and *sos-1* were consistently induced upon treatment with *O. cornuta*, indicating their contribution to the response following *O. cornuta* treatment (Figure 6A, 2.53-fold induction over the control in *mek-2* expression, P=0.0006; 6.86-fold induction in *sos-1* expression, P=0.0002 by two-tailed Mann–Whitney test (30)). Likewise, other players in the MAPK pathway, such as *let-60* (Ras) and *mpk-1* (MAP kinase), were also significantly induced, further validating the activation of the MAPK pathway in response to *O. cornuta* treatment (1.74-fold induction over the control in *mpk-1* expression, P=0.0003; 1.43-fold induction in *let-60* expression, P=0.0003).

Preprints.org (www.preprints.org) | NOT PEER-REVIEWED | Posted: 4 December 2023 doi:10.20944/preprints202312.0154.v1

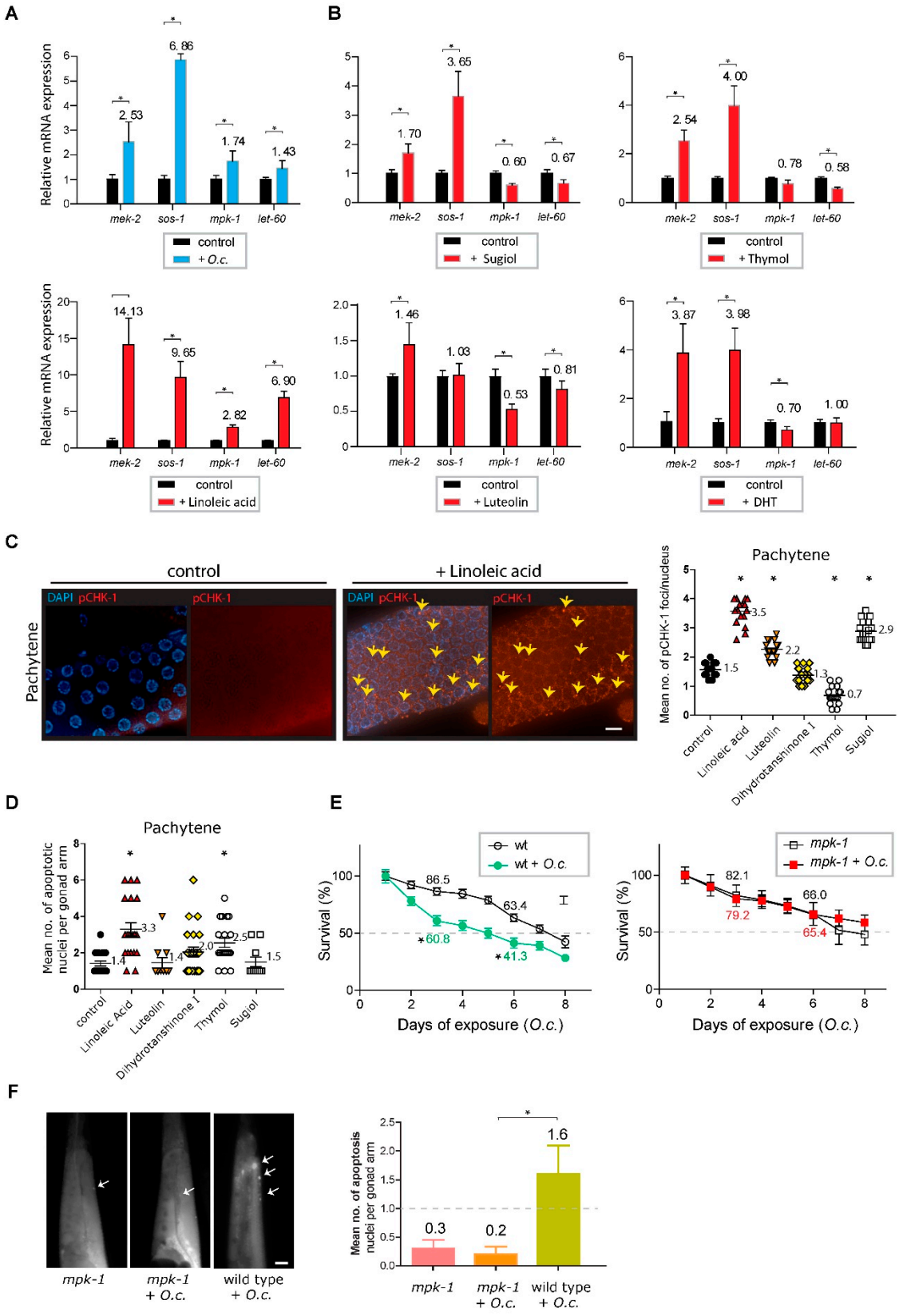

Figure 6. MAPK pathway activation and its role in response to *O. Cornuta* treatment. (A) Induction of the MAPK pathway components *mek-2* and *sos-1* upon *O. cornuta* treatment. *mek-2* expression increased by 2.53-fold (P=0.0006), and *sos-1* expression increased by 6.86-fold (P=0.0002) compared to the control. Additionally, *mpk-1* and *let-60* expression was induced by 1.74-fold (P=0.0003) and 1.43-fold (P=0.0003), respectively. Asterisks indicate statistical significance by the two-tailed Mann–

 doi:10.20944/preprints202312.0154.v1

Whitney test. **(B)** Activation of the MAPK pathway by individual compounds in *O. cornuta.* For instance, sugiol treatment increased *mek-2* expression by 1.7-fold (P=0.0002) and *sos-1* expression by 3.65-fold (P=0.0002). Thymol treatment resulted in a 2.54-fold increase in *mek-2* expression (P=0.0009) and a 4.0-fold increase in *sos-1* expression (P=0.0009). Intriguingly, linoleic acid induced all four MAPK components, while other compounds induced one or two genes. Various *O. cornuta* compounds (sugiol, thymol, linoleic acid, luteolin, and DHT) altered MAPK pathway expression. DHT (Dihydrotanshinone). **(C)** Linoleic acid-induced DNA damage checkpoint activation. Increased pCHK-1 foci during the pachytene stage (P<0.0001). Arrows indicate pCHK-1 foci. Asterisks indicate statistical significance against the control group. Bar=2 μm. **(D)** Linoleic acid-triggered apoptosis in germline nuclei similar to *O. cornuta* treatment (P<0.0001). Other *O. cornuta* compounds did not show a simultaneous increase in both pCHK-1 foci and apoptosis. Asterisks indicate statistical significance against the control group. **(E)** The role of the MAPK pathway in the *O. cornuta* response validated by the *mpk-1(ga111)* mutant strain. Reduced survivability was reversed in the mutant (P=0.4256 on day 5, P=0.4208 on day 10 by the two-tailed t test). Relative survivability is presented. Asterisks indicate statistical significance against the control group. (F) Suppressed apoptosis in the *mpk-1 (ga111)* mutant, supporting MAPK-dependent DNA damage pathway activation and survivability (P=0.0173 in *mpk-1 +O.c.* and wild type +*O.c.*). Arrows indicate nuclei undergoing apoptosis. Asterisks indicate statistical significance against the control group. Bar=20 μm.

Since *O. cornuta* comprises multiple anticancer compounds, we further tested how these compounds in *O. cornuta* function in DNA damage repair. Intriguingly, all five compounds led to the upregulation of *mek-2*, and four of them induced the expression of *sos-1,* suggesting that the majority of these compounds are involved in activating the MAPK pathway (Figure 6B). For instance, under sugiol treatment, *mek-2* expression increased 1.7-fold over the control (P=0.0002), and *sos-1* expression rose 3.65-fold (P=0.0002). Likewise, with thymol treatment, *mek-2* expression showed a 2.54-fold increase over the control (P=0.0009), and *sos-1* expression increased 4-fold (P=0.0009).

Provocatively, linoleic acid induced all four MAPK components, while the other four compounds reduced one or two genes. This implies an unequal contribution of these compounds to the phenotypes in the *O. cornuta* extract (Figure 6B). Specifically, we observed significant increases: 14.13-fold in *mek-2* (P=0.0016), 9.65-fold in *sos-1* (P=0.0007), 2.82-fold in *mpk-1* (P=0.0002), and 6.9-fold in *let-60* expression (P=0.0003).

Given that the expression pattern of linoleic acid is similar to that of *O. cornuta* extracts across four MAPK genes, we explored whether linoleic acid could induce the meiotic defects and activate DNA damage checkpoints observed in *O. cornuta* treatment. Notably, linoleic acid treatment prompted the activation of the DNA damage checkpoint, as evidenced by the increased presence of pCHK-1 foci during the pachytene stage (Figure 6C, 1.5 vs 3.5 in control and linoleic acid, P<0.0001). This activation of the DNA damage checkpoint consequently triggered apoptosis in germline nuclei, mirroring the observations from *O. cornuta* treatment (Figure 6D, 1.4 vs 3.3 in control and linoleic acid, P<0.0001). In contrast, among the other four compounds extracted from *O. cornuta*, none demonstrated a simultaneous increase in both pCHK-1 foci and apoptosis. This observation suggests that the phenotypic effects present in *O. cornuta* are uniquely represented by linoleic acid.

The elevated expression of multiple MAPK pathway components suggests a pivotal role for the MAPK pathway in response to *O. cornuta* treatment. We further examined whether the MAPK pathway is indeed responsible for the phenotypes exhibited upon *O. cornuta* exposure. To explore this connection, we employed the *mpk-1(ga111)* mutant strain, which exhibits a potential deficiency in MEK activation in the context of *O. cornuta* exposure (32). In alignment with our mRNA expression data, defective MEK activation reversed the reduction in survivability, highlighting the substantial involvement of the MAPK pathway in the response to *O. cornuta* treatment (Figure 6E). While *O. cornuta* treatment significantly decreased the survival rate of wild-type worms (86.5 vs. 60.8 on day 3, P=0.0015; 63.4 vs. 41.3 on day 6, P=0.0077), the *mpk-1* mutants showed no marked difference compared to the control groups (82.1 vs. 79.2 on day 3, P=0.3962; 66.0 vs. 65.4 on day 6, P=0.4799 by the two-tailed t test).

 doi:10.20944/preprints202312.0154.v1

Moreover, this mutant exhibited a suppressed level of apoptosis, further supporting the idea of MAPK pathway-dependent DNA damage pathway activation and survivability upon *O. cornuta* exposure (Figure 6F, 0.2 vs 1.6 in *mpk-1(ga111)* +*O.c.* and wild type/N2 +*O.c.*, P=0.0173). All these observations suggest that the MAPK pathway is indispensable for proper survival; therefore, losing MEK activation eliminates the reduction in survival. In summary, our data collectively demonstrated that various constituents of the *O. cornuta* extract enhance MAPK pathway elements and impact worm survival through this pathway. Notably, linoleic acid emerges as a significant player in this intricate process.

Discussion

This study leveraged *C. elegans* to assess the potential nematocidal toxicity of herbal extracts and elucidated their roles in DNA damage repair and checkpoint responses. A screen of 316 herb extracts identified *O. cornuta* and *V. lobelianum* as activators of DNA damage checkpoint responses, DNA damage apoptosis, high incidence of males (HIM), defective meiotic progression, and reduced survival rates. Strikingly, while *V. lobelianum* downregulated hedgehog expression, *O. cornuta*, containing numerous anticancer compounds, upregulated the MAPK pathway, suggesting that distinct pathways mediate the reduced survival and DNA damage checkpoint response. Moreover, defects in the MAPK pathway abolished the phenotypes exhibited in *O. cornuta* exposure (Figure 6F), supporting the idea that MAPK-dependent survivability and DNA damage checkpoint activation play a crucial role in *O. cornuta* treatment.

V. lobelianum

Veratrum lobelianum Bernh. (Melanthiaceae), a hardy herbaceous plant primarily found across Northeast Asia, Central Europe, and North America (33), has been associated with toxicity in both humans and animals. Jervine, an abundant alkaloid in *V. lobelianum*, has demonstrated its ability to exert antitumor effects and influence DNA damage repair processes in nasopharyngeal carcinoma cells (24, 27, 34). Our findings align with a prior report in which jervine was shown to induce apoptosis by blocking the Hedgehog signaling pathway in nasopharyngeal cancer cells (27). In our experiments, treatment with jervine-containing *V. lobelianum* extract activated the DNA damage checkpoint by downregulating hedgehog signaling (Figure 3 and 4). While it is plausible that the downregulation of hedgehog is attributed to the presence of jervine in the herb extract, jervine itself upregulates Hedgehog expression, suggesting that the observed phenotypes in *V. lobelianum* may not solely stem from jervine (Figure 5B). Furthermore, the fact that jervine did not induce pCHK-1 or DNA damage-induced germline apoptosis provides additional support for this idea (Figure 5C and 5D, respectively).

The observed discrepancy may be attributed to different organisms: humans vs. nematodes. However, it is worth noting that a similar discrepancy has also been reported in other mammalian studies. For instance, research has shown that *Veratrum album* extract can protect against radiotherapy-induced gastrointestinal toxicity (35), indicating that herbal extracts containing jervine may have distinct roles compared to jervine alone. With over one hundred alkaloids in Veratrum species, other compounds present in *V. lobelianum* may contribute to nematocidal toxicity, including protoveratrine A and B, which have been implicated in conditions such as arterial hypertension, sleep apnea, and emetic responses (33, 36, 37). Further studies are needed to fully understand the impact of alkaloids on nematodes or humans, as well as the collaborative actions within *V. lobelianum* that may lead to synergistic nematode toxicity. Comparative studies on alkaloid combinations and concentrations have the potential to optimize applications such as cancer treatment.

O. cornuta

Onobrychis cornuta (L.) Desv. (Fabaceae), found in the mountainous regions of Iran-Turan and Turkey, has traditionally employed its flowers and seeds in medicinal practices (38, 39). This plant is

 doi:10.20944/preprints202312.0154.v1

recognized for its resilience to high temperatures, aridity, diseases, and wireworms such as *Dipsosphecia scopigera* and *Sphenoptera carceli*, although the underlying mechanism remains uncertain.

In parallel with *V. lobelianum*, *O. cornuta* extracts resulted in diminished %survival and %adult rates (Figure 2B) and exhibited impaired meiotic progression (Figure 5). The notable increase in pCHK-1 foci count and elevated apoptosis levels in the pachytene germline indicate an apoptotic pathway triggered by DNA damage. These findings collectively underscore the potential of *O. cornuta* extracts as promising candidates for antitumor drug development.

Remarkably, extracts from *O. cornuta* encompass multiple pro-apoptotic compounds, with nine out of thirteen major compounds implicated in anticancer effects (Table 1). LC–MS analysis of the *O. cornuta* herb yields highly significant and promising results, suggesting the presence of numerous compounds with potential anticancer properties. Linoleic acid, a vital omega-6 polyunsaturated fatty acid, recapitulated phenotypes induced by *O. cornuta* exposure, including elevated pCHK-1 foci levels, apoptosis, and MAPK pathway activation.

Linoleic acid plays a pivotal role in various physiological processes, encompassing cell membrane structure and function. While autoxidized linoleic acid can cause DNA strand breaks in plasmid DNA and human lymphocytes and fibroblasts (40-43), it also functions protectively by counteracting DNA damage and apoptosis induced by substances such as palmitic acid (44). This dual nature underscores the importance of meticulous analysis to fully comprehend linoleic acid's intricate impacts on both health and cellular processes.

While some hedgehog players were upregulated by *O. cornuta* exposure, treatment with *O. cornuta* induced the expression of MEK-2 and SOS-1, components of the MAPK pathway. SOS-1 serves as a putative guanine nucleotide exchanger for LET-60 ras (45), facilitating the exchange of GDP for GTP on Ras proteins and activating them. Overexpressing GEF leads to elevated Ras signaling pathway activity. The expression of LET-60/Ras and MPK-1/MAP kinase was also stimulated, further validating the activation of the MAPK pathway due to *O. cornuta* treatment (Figure 6 and Figure 7).

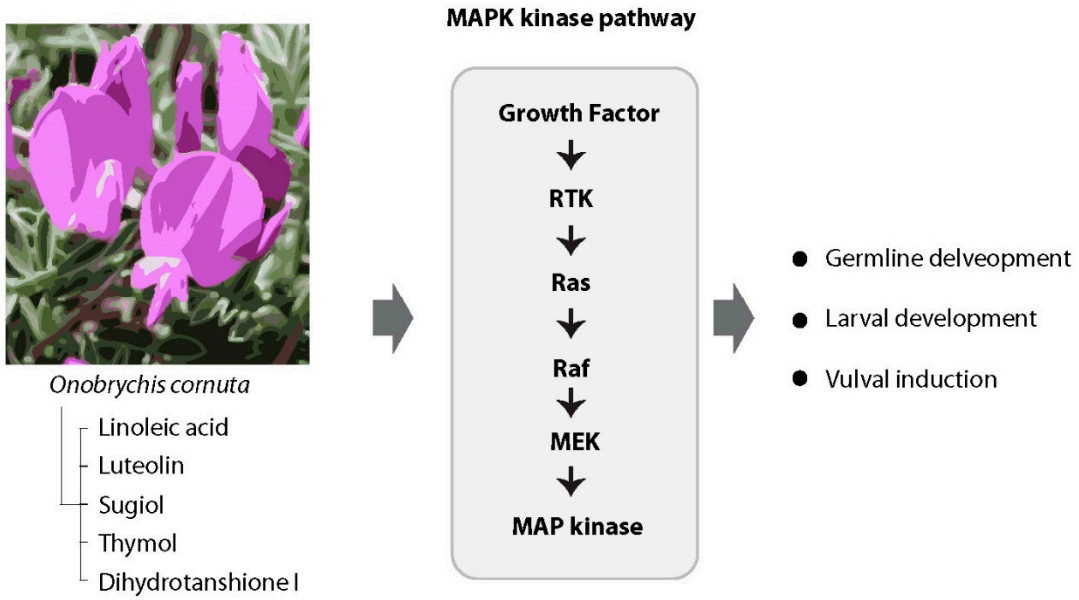

Figure 7. *O. Cornuta* extract induces an upregulation of the MAPK kinase pathway, resulting in germline abnormalities and influencing worm survival. Our observation highlights that not only does *O. cornuta* itself lead to the upregulation of the MAPK pathway, but the compounds within the *O. cornuta* extract also play a significant role in this process. This collective activation of the MAPK pathway underscores its pivotal involvement in influencing germline abnormalities and impacting worm survival.

 doi:10.20944/preprints202312.0154.v1

Our findings align with existing knowledge, as the two genes involved in the Let-60/Ras-mediated MAPK pathway play pivotal roles in proper germline development (30). This underscores the significance of MAPK in *O. cornuta* treatment responses. Notably, gain-of-function *mek-2* alleles induced pleiotropic defects, including embryonic lethality and a multiple vulva (Muv) phenotype, while loss-of-function alleles suppressed the phenotype (Figure 7, (30)). Likewise, the *mpk-1 (ga111) mutant*, defective in MEK activation (32), suppressed the reduced survivability and higher level of apoptosis observed under *O. cornuta* exposure, indicating the role of the MAPK pathway in defective germline progression and DNA damage checkpoint response activation (Figure 6E and 6F). Collectively, our results indicate that *O. cornuta*-induced MAPK pathway overexpression leads to abnormal meiotic development and reduced survivability. Encouragingly, the five major *O. cornuta* compounds upregulate MEK-2 and SOS-1. Subsequent studies on the MAPK pathway should aim to uncover how *O. cornuta* upregulates this pathway.

V. lobelianum and O. cornuta Herbal Extracts: Balancing Promise and Toxicity

While herbal extracts from *V. lobelianum* and *O. cornuta* show promise as novel antitumor drugs by halting the cell cycle, they also exhibit toxicity to noncancerous cells. For instance, in lambs, Veratrum ingestion causes birth defects, including craniofacial issues (46). Similarly, our research indicates that both extracts disrupt meiotic processes during germline nuclei development (Figure 2), indicating flaws in meiotic development in *C. elegans* (47, 48).

Interestingly, exposure to *O. cornuta* prompts an intriguing rise in the MAPK pathway, leading to hindered meiotic progression. This impact of *O. cornuta* on the MAPK pathway has significant implications for scientific study and potential drug development. Activating this pathway could offer a valuable tool for in-depth exploration of cellular signaling mechanisms, aiding the identification of therapeutic targets for various diseases.

Our data strongly support the involvement of the MAPK pathway in *O. cornuta*'s effects, further supported by LC–MS analysis revealing anticancer compounds in *O. cornuta* extracts. Compounds of *O. cornuta* extracts and the O. cornuta extract *per se* stimulate critical components of the MAPK pathway, reinforcing its role in germline development.

Despite discovering thirteen noteworthy compounds within *O. cornuta*, nine known for their anticancer properties, the precise ways they affect the MAPK pathway require further elucidation. Comparing *V. lobelianum* and *O. cornuta* extracts highlights differences in their molecular mechanisms and signaling pathways that eventually produced similar output: DNA damage apoptosis and defective germline development. The use of the mutant strain, which displays reduced MEK activation, provides compelling evidence for the central importance of the MAPK pathway in the abnormal effects induced by *O. cornuta.*

This study presents a compelling array of evidence highlighting the potential antitumor effects stemming from extracts from *O. cornuta* and *V. lobelianum*. These effects can be attributed to their notable influence on critical processes linked to DNA damage repair, activation of DNA damage checkpoint responses, and their skillful modulation of the MAPK pathway. However, the weight of these findings demands a tempered approach, urging us to tread cautiously due to conceivable toxicity concerns in noncancerous cells. The intricate interplay observed among the various compounds within these herbal extracts emphasizes the magnitude of our discoveries. Their multifaceted impact on cellular processes underscores the paramount importance of our findings in the broader landscape of scientific understanding.

The discovery of linoleic acid within *O. cornuta* and Jervine in *V. lobelianum* sheds light on specific constituents likely contributing to the observed antitumor properties. As such, both *V. lobelianum* and *O. cornuta* stand out as promising resources in developing potential antitumor drugs. The promising trajectory of these herbal extracts begs the way for further exploration and investigation into the constituent elements, hinting at the potential for revolutionary therapeutic strategies to emerge within the realm of cancer treatment.

Materials and Methods

 doi:10.20944/preprints202312.0154.v1

Strains and alleles

All *C. elegans* strains were cultured at 20°C under standard conditions as described, and the N2 Bristol strain was used as the wild-type.

Herb extraction

Veratrum lobelianum and *Onobrychis cornuta* were collected in Armenia in May 2006. Plant material was freed of extraneous matter, air-dried in the shade, milled to a coarse powder and extracted with methanol. The pooled methanol extract was concentrated *in vacuo* to afford a tarry residue. The methanol extract was dissolved in 90% (aqueous) methanol and extracted with n-hexane. The residual hydroalcoholic phase was freed of the solvent *in vacuo*, suspended in water, and then sequentially extracted with dichloromethane and n-butanol (n-BuOH) to afford a gross separation into hexane-, dichloromethane-, butanol-, and water-soluble fractions. The resulting extracts were dissolved in DMSO, diluted to a final concentration of 1 mg/ml in DMSO, and subsequently further diluted using M9 buffer to achieve a final concentration of 0.03 μg/ml. Three solvents, hexane, butanol, and water, were designated -H, -B, and -A, respectively.

Survival, larval arrest/lethality and HIM

Gravid hermaphrodites were collected from NGM plates to establish synchronized L1 stage larvae, following the protocol outlined in (19, 49). These synchronized worms were then suspended in 180 μl of the herb extract solution and transferred to a 96-well plate. Subsequently, the worms were gently agitated and incubated at 20°C for 24 hours. Phenotypic changes were monitored continuously, extending up to 48 hours.

To assess relative survival, the worms' mobility was monitored after 24 hours of incubation. The brood sizes represent the total number of eggs laid by each individual worm during the 4-5 days following the L4 stage. Larval arrest or lethality indicates the percentage of hatched worms that did not survive to reach adulthood. Additionally, the proportion of males in the population (%Him) was calculated, representing the percentage of adult worms that were males.

For each reported generation, an analysis was conducted on the entire progeny of approximately 20 worms for each genotype. Statistical comparisons between different genotypes were carried out using the two-tailed Mann–Whitney test with a 95% confidence interval (C.I.). All experiments were performed in triplicate to ensure reproducibility.

Cumulative survival

At least 60 L4 stage worms were collected for the assessment of survivability. Chemical solutions were prepared by diluting them with M9 buffer. The concentration of linoleic acid in these solutions was maintained at 0.3 μM, as referenced in (50).

The procedure for the survivability study was adopted from the work of Kim and Colaiacovo (49). L4 stage worms were gathered and placed in a 24-well plate along with the appropriately diluted chemical solutions. Incubation was carried out at a temperature of 20°C overnight. After incubation, the worms underwent three rounds of rinsing with M9 buffer to remove residual chemicals from their exteriors. Subsequent to the rinsing process, the worms were transferred onto NGM plates, with each plate accommodating 20 worms. Three replicates were prepared for each treatment. The survival rates of the worms were monitored for 10 days. On a daily basis, any surviving worms were moved to fresh NGM plates following the counting procedure.

Preparation of worm lysates for mass spectrometric analysis

Worm preparation methods for LC–MS analysis were described in (51). Age-matched worms (20 hours post-L4) were exposed to M9 buffer with different herb extracts (0.03 μg/ml) at 25°C for 20 hours. After exposure, worms were washed 10 times in M9 buffer and frozen with minimal M9 in liquid nitrogen. The worm pellet was resuspended in lysis buffer (0.5 M sucrose, 25 mM HEPES (pH

 doi:10.20944/preprints202312.0154.v1

7.6), 5 mM EDTA, 0.5% CHAPS, 0.5% deoxycholic acid). Samples were homogenized and centrifuged to remove worm fragments. LC–MS was performed by YanBo times (Beijing, China).

LC–MS analysis

The LC–MS/MS method used in this study employed a Shimadzu LC-30A chromatography system with a C18 column (2.2 μm, 2.1x100 mm). The column temperature was maintained at 40°C, and the flow rate was set at 0.2 ml/min. A 2 μL sample was injected onto the column. The mobile phase consisted of acetonitrile and 0.1% formic acid solution. The mass spectrometry instrument used was the AB Sciex Triple TOF 5600+. For the positive ionization mode, the ion source voltage was 5500 V, and the ion source temperature was set to 500°C. The declustering potential (DP) was set at 100 V, collision energy (CE) at 40 eV, and collision energy spread (CES) at 15 eV. Nitrogen gas was used as the nebulizing gas, with 50 PSI for both auxiliary gases 1 and 2 and 40 PSI for the curtain gas. The mass spectrometer performed first-level MS scanning in the range of 100-1500 m/z, followed by second-level MS scanning for peaks with a response greater than 100 cps. The range for second-level MS scanning was also set at 100-1500 m/z, and dynamic background subtraction (DBS) was enabled. For the negative ionization mode, the ion source voltage was set at -4500 V, and all other parameters remained the same as in the positive ionization mode.

Monitoring the growth of E. coli

The growth performance of *E. coli* OP50 in different herb extracts was analyzed by optical density as described in (52). To test whether the herb extracts show any antibacterial impact against *E. coli* OP50, the bacterial growth was determined by frequently measuring the optical density (at 600 nm) during exposure to 0.03 μg/ml of each herb extract (53).

Immunofluorescence staining

Whole-mount preparations of dissected gonads, fixation and immunostaining procedures were carried out as described in (54). Primary antibodies were used at the following dilutions: rabbit pCHK-1 (1:250, Cell Signaling, Ser345). The secondary antibodies used were Cy3 anti-rabbit (1:300) from Jackson Immunochemicals. Immunofluorescence images were collected at 0.2 μm intervals with an Eclipse Ti2-E inverted microscope and a DSQi2 camera (Nikon). Photos were taken with a 60x objective combined with 1.5x auxiliary magnification and were subjected to deconvolution using NIS Elements software (Nikon). Partial projections of half nuclei are shown.

Quantitative analysis of pCHK-1 foci

Quantitation of pCHK-1 foci was performed as described in (54). Between five and ten germlines were scored for each treatment. Statistical comparisons between treatments were performed using the two-tailed Mann–Whitney or T test with a 95% confidence interval.

Quantitation of germline apoptosis

Germlines of age-matched (20 hours post-L4) animals were analyzed by acridine orange staining, as described in (55), utilizing a Nikon Ti2-E fluorescence microscope. Between 20 and 30 gonads were scored for each treatment. Statistical comparisons between treatments were performed using the two-tailed Mann–Whitney test, 95% C.I.

Acknowledgments: We thank members of the Kim laboratory for discussions and proofreading. This work was funded by the Kunshan Shuangchuang grant award (KSSC202202060) and the National Natural Science Foundation of China grant (NSFC No. 31972876) to H.-M.K. Some strains were provided by the CGC, which is funded by the NIH Office of Research Infrastructure Programs (P40 OD010440).

References

 doi:10.20944/preprints202312.0154.v1

1. Report MA. Medical Foods Market Size, Share & Trends Analysis Report By Route of Administration (Oral, Enteral), By Product (Pills, Powder, Liquid), By Application, By Sales Channel, And Segment Forecasts, 2022 - 2030. 2020.
2. Shaul NC, Jordan JM, Falsztyn IB, Baugh LR. Insulin/IGF-dependent Wnt signaling promotes formation of germline tumors and other developmental abnormalities following early-life starvation in Caenorhabditis elegans. Genetics. 2022.
3. Lui DY, Colaiacovo MP. Meiotic development in Caenorhabditis elegans. Advances in experimental medicine and biology. 2013;757:133-70.
4. Duronio RJ, O'Farrell PH, Sluder G, Su TT. Sophisticated lessons from simple organisms: appreciating the value of curiosity-driven research. Disease models & mechanisms. 2017;10(12):1381-9.
5. Wang Q, Yang F, Guo W, Zhang J, Xiao L, Li H, et al. Caenorhabditis elegans in Chinese medicinal studies: making the case for aging and neurodegeneration. Rejuvenation Res. 2014;17(2):205-8.
6. Matsunami K. Frailty and Caenorhabditis elegans as a Benchtop Animal Model for Screening Drugs Including Natural Herbs. Front Nutr. 2018;5:111.
7. Choi J, Ahn A, Kim S, Won CW. Global Prevalence of Physical Frailty by Fried's Criteria in Community-Dwelling Elderly With National Population-Based Surveys. J Am Med Dir Assoc. 2015;16(7):548-50.
8. David DC, Ollikainen N, Trinidad JC, Cary MP, Burlingame AL, Kenyon C. Widespread protein aggregation as an inherent part of aging in C. elegans. PLoS Biol. 2010;8(8):e1000450.
9. Moliner C, López V, Barros L, Dias MI, Ferreira IC, Langa E, et al. Rosemary flowers as edible plant foods: phenolic composition and antioxidant properties in Caenorhabditis elegans. Antioxidants. 2020;9(9):811.
10. Sayed SM, Siems K, Schmitz-Linneweber C, Luyten W, Saul N. Enhanced Healthspan in Caenorhabditis elegans Treated With Extracts From the Traditional Chinese Medicine Plants Cuscuta chinensis Lam. and Eucommia ulmoides Oliv. Frontiers in Pharmacology. 2021;12:604435.
11. Anjaneyulu J, Vidyashankar R, Godbole A. Differential effect of Ayurvedic nootropics on C. elegans models of Parkinson's disease. Journal of Ayurveda and Integrative Medicine. 2020;11(4):440-7.
12. Hodgkin J, Horvitz HR, Brenner S. Nondisjunction Mutants of the Nematode CAENORHABDITIS ELEGANS. Genetics. 1979;91(1):67-94.
13. Cinquin O, Crittenden SL, Morgan DE, Kimble J. Progression from a stem cell-like state to early differentiation in the C. elegans germ line. Proc Natl Acad Sci U S A. 2010;107(5):2048-53.
14. Dernburg AF, McDonald K, Moulder G, Barstead R, Dresser M, Villeneuve AM. Meiotic recombination in C. elegans initiates by a conserved mechanism and is dispensable for homologous chromosome synapsis. Cell. 1998;94(3):387-98.
15. Gisselsson D. Classification of chromosome segregation errors in cancer. Chromosoma. 2008;117(6):511-9.
16. Csankovszki G, Collette K, Spahl K, Carey J, Snyder M, Petty E, et al. Three distinct condensin complexes control C. elegans chromosome dynamics. Curr Biol. 2009;19(1):9-19.
17. Girard C, Roelens B, Zawadzki KA, Villeneuve AM. Interdependent and separable functions of Caenorhabditis elegans MRN-C complex members couple formation and repair of meiotic DSBs. Proc Natl Acad Sci U S A. 2018;115(19):E4443-E52.
18. Hofmann ER, Milstein S, Boulton SJ, Ye M, Hofmann JJ, Stergiou L, et al. Caenorhabditis elegans HUS-1 is a DNA damage checkpoint protein required for genome stability and EGL-1-mediated apoptosis. Curr Biol. 2002;12(22):1908-18.
19. Kim HM, Colaiacovo MP. ZTF-8 Interacts with the 9-1-1 Complex and Is Required for DNA Damage Response and Double-Strand Break Repair in the C. elegans Germline. PLoS Genet. 2014;10(10):e1004723.
20. Marechal A, Zou L. DNA damage sensing by the ATM and ATR kinases. Cold Spring Harb Perspect Biol. 2013;5(9).
21. Kim HM, Colaiacovo MP. New Insights into the Post-Translational Regulation of DNA Damage Response and Double-Strand Break Repair in Caenorhabditis elegans. Genetics. 2015;200(2):495-504.
22. Gartner A, Milstein S, Ahmed S, Hodgkin J, Hengartner MO. A conserved checkpoint pathway mediates DNA damage--induced apoptosis and cell cycle arrest in C. elegans. Mol Cell. 2000;5(3):435-43.
23. Rahman a, Choudhary. New Steroidal Alkaloids from Rhizomes of Veratrum album. Journal of Natural Products 1992;55:565-70.
24. Taldaev A, Terekhov RP, Melnik EV, Belova MV, Kozin SV, Nedorubov AA, et al. Insights into the Cardiotoxic Effects of Veratrum Lobelianum Alkaloids: Pilot Study. Toxins. 2022;14(7):490.
25. Tang J, Li HL, Shen YH, Jin HZ, Yan SK, Liu XH, et al. Antitumor and antiplatelet activity of alkaloids from veratrum dahuricum. Phytother Res. 2010;24(6):821-6.
26. Tang J, Li HL, Shen YH, Jin HZ, Yan SK, Liu RH, et al. Antitumor activity of extracts and compounds from the rhizomes of Veratrum dahuricum. Phytother Res. 2008;22(8):1093-6.
27. Chen J, Wen B, Wang Y, Wu S, Zhang X, Gu Y, et al. Jervine exhibits anticancer effects on nasopharyngeal carcinoma through promoting autophagic apoptosis via the blockage of Hedgehog signaling. Biomedicine & Pharmacotherapy. 2020;132:110898.
28. Burglin TR, Kuwabara PE. Homologs of the Hh signalling network in C. elegans. WormBook. 2006:1-14.

 doi:10.20944/preprints202312.0154.v1

29. Raleigh DR, Reiter JF. Misactivation of Hedgehog signaling causes inherited and sporadic cancers. J Clin Invest. 2019;129(2):465-75.
30. Wu Y, Han M, Guan KL. MEK-2, a Caenorhabditis elegans MAP kinase kinase, functions in Ras-mediated vulval induction and other developmental events. Genes Dev. 1995;9(6):742-55.
31. Zhang W, Liu HT. MAPK signal pathways in the regulation of cell proliferation in mammalian cells. Cell Res. 2002;12(1):9-18.
32. Lackner MR, Kim SK. Genetic analysis of the Caenorhabditis elegans MAP kinase gene mpk-1. Genetics. 1998;150(1):103-17.
33. W.-J. Liao Y-MYaD-YZ. Biogeography and evolution of flower color in Veratrum (Melanthiaceae) through inference of a phylogeny based on multiple DNA markers. Pl Syst Evol 2007;267:177-90.
34. Melnik E, Belova M, Tyurin I, Ramenskaya G. Quantitative Content Parameter in the Standardization of Veratrum Aqua, Veratrum Lobelianum Bernh. Based Drug. Drug development & registration. 2021;10(1):107-13.
35. Yakan S, Aydin T, Gulmez C, Ozden O, Eren Erdogan K, Daglioglu YK, et al. The protective role of jervine against radiation-induced gastrointestinal toxicity. Journal of Enzyme Inhibition and Medicinal Chemistry. 2019;34(1):789-98.
36. Zomlefer WB, Williams NH, Whitten WM, Judd WS. Generic circumscription and relationships in the tribe Melanthieae (Liliales, Melanthiaceae), with emphasis on Zigadenus: evidence from ITS and trnL-F sequence data. Am J Bot. 2001;88(9):1657-69.
37. ZOMLEFER W, WILLIAMS, JUDD. An Overview of Veratrum s.l. (Liliales: Melanthiaceae) and an Infrageneric Phylogeny Based on ITS Sequence Data. Systematic Botany. 2003;28(2):250-69.
38. Erkovan HI, Mehmet Kerim Gullap, Şule Erkovan and Ali Koç. HORNED SAINFOIN (ONOBRYCHIS CORNUTA (L.) DESV.): IS IT AN AMUSING OR NUISANCE PLANT FOR STEPPE RANGELANDS? Ecology & Safety. 2016;10:418-23.
39. Joudi LaGHB. Exploration of medicinal species of Fabaceae, Lamiaceae and Asteraceae families in Ilkhji region, Eastern Azerbaijan Province (Northwestern Iran). Journal of Medicinal Plants Research. 2010;4:1081-4.
40. Burcham PC. Genotoxic lipid peroxidation products: their DNA damaging properties and role in formation of endogenous DNA adducts. Mutagenesis. 1998;13(3):287-305.
41. Inouye S. Site-specific cleavage of double-strand DNA by hydroperoxide of linoleic acid. FEBS Lett. 1984;172(2):231-4.
42. Kodama TNMKM. Detection of DNA Damage in Cultured Human Fibroblasts Induced by Methyl Linoleate Hydroperoxide. Agric Biol Chem 1986;50(1):261-2.
43. Ueda K, Kobayashi S, Morita J, Komano T. Site-specific DNA damage caused by lipid peroxidation products. Biochim Biophys Acta. 1985;824(4):341-8.
44. Beeharry N LJ, Hernandez AR, Chambers JA, Fucassi F, Cragg PJ, Green MH, Green IC. Linoleic acid and antioxidants protect against DNA damage and apoptosis induced by palmitic acid. Mutat Res 2003;530(1-2):27-33.
45. Chang C, Hopper NA, Sternberg PW. Caenorhabditis elegans SOS-1 is necessary for multiple RAS-mediated developmental signals. EMBO J. 2000;19(13):3283-94.
46. Lee ST, Panter KE, Gaffield W, Stegelmeier BL. Development of an enzyme-linked immunosorbent assay for the veratrum plant teratogens: cyclopamine and jervine. J Agric Food Chem. 2003;51(3):582-6.
47. Ren X, Tian S, Meng Q, Kim HM. Histone Demethylase AMX-1 Regulates Fertility in a p53/CEP-1 Dependent Manner. Front Genet. 2022;13:929716.
48. Zhang X, Tian S, Beese-Sims SE, Chen J, Shin N, Colaiacovo MP, et al. Histone demethylase AMX-1 is necessary for proper sensitivity to interstrand crosslink DNA damage. PLoS Genet. 2021;17(7):e1009715.
49. Kim HM, Colaiacovo MP. DNA Damage Sensitivity Assays in Caenorhabditis elegans. Bio-Protocol. 2015;5(11).
50. Webster CM, Deline ML, Watts JL. Stress response pathways protect germ cells from omega-6 polyunsaturated fatty acid-mediated toxicity in Caenorhabditis elegans. Dev Biol. 2013;373(1):14-25.
51. Shin N, Cuenca L, Karthikraj R, Kannan K, Colaiacovo MP. Assessing effects of germline exposure to environmental toxicants by high-throughput screening in C. elegans. PLoS Genet. 2019;15(2):e1007975.
52. Sayed SMA, Siems K, Schmitz-Linneweber C, Luyten W, Saul N. Enhanced Healthspan in Caenorhabditis elegans Treated With Extracts From the Traditional Chinese Medicine Plants Cuscuta chinensis Lam. and Eucommia ulmoides Oliv. Front Pharmacol. 2021;12:604435.
53. Penuelas-Urquides K, Villarreal-Trevino L, Silva-Ramirez B, Rivadeneyra-Espinoza L, Said-Fernandez S, de Leon MB. Measuring of Mycobacterium tuberculosis growth. A correlation of the optical measurements with colony forming units. Braz J Microbiol. 2013;44(1):287-9.
54. Colaiacovo MP, MacQueen AJ, Martinez-Perez E, McDonald K, Adamo A, La Volpe A, et al. Synaptonemal complex assembly in C. elegans is dispensable for loading strand-exchange proteins but critical for proper completion of recombination. Dev Cell. 2003;5(3):463-74.

 doi:10.20944/preprints202312.0154.v1

55. Kelly KO, Dernburg AF, Stanfield GM, Villeneuve AM. Caenorhabditis elegans msh-5 is required for both normal and radiation-induced meiotic crossing over but not for completion of meiosis. Genetics. 2000;156(2):617-30.
56. Carvalho A, Olson SK, Gutierrez E, Zhang K, Noble LB, Zanin E, et al. Acute drug treatment in the early C. elegans embryo. PLoS One. 2011;6(9):e24656.